Iranian Journal of Geophysics, Vol 20 No 3, 2026, Page 43 – 63 (Research Article)
DOI: 10.30499/ijg.2025.500189.1666

Exploration and resource evaluations of mineral using modeling and GPR applications: case study in Morocco

Mohammed Hamdaoui[1*], faize Ahmed[1] and Sara Said [2]

[1]Ph.D., Mathematics and Information Systems Laboratory, Faculty of Polydisciplinary Studies of Nador, Mohammed First University, Oujda, Morocco
[2] Ph.D., Department Research Center, High Studies of Engineering School (EHEI), Oujda, Morocco

(Received: 23 January 2025, Accepted: 04 May 2025)

Abstract

This paper presents a contemporary methodology for mineral research and exploration, with a particular focus on iron ores and geophysical mapping in the Nador region of eastern Morocco. The application of Ground Penetrating Radar (GPR) in the exploration of subsurface objects and minerals has demonstrated significant success and efficacy. GPR technology has emerged as a powerful, non-destructive tool for the exploration and resource assessment of minerals. One of the primary objectives of this study is to utilize geophysical mapping to identify the locations and quantities of mineral deposits for future exploitation and exploration. To interpret the data and results obtained from GPR, we employed modeling techniques to simulate GPR signals for the detection of various minerals using the GprMax2d software. The algorithm underpinning this program has been enhanced to improve its effectiveness and accuracy in detecting targets and determining their physical properties. This study leveraged the simulation and modeling to interpret data and compare the amplitude of reflected signals from the surfaces of different objects and minerals.

Keywords: Ground penetrating radar (GPR), exploration, non-destructive method, mineral, subsurface mapping, modeling, Morocco

*Corresponding author: hamdawimohammedpc@gmail.com

1 Introduction

Ground Penetrating Radar (GPR) is a non-invasive geophysical technique that has gained prominence in mining, mineral prospecting, and resource assessment. Its ability to provide high-resolution subsurface imaging has made it valuable in civil engineering, geophysics, and archaeology [1,2]. Research by Francke (2012) and Cheng (2004) has confirmed GPR's effectiveness in mineral detection [3,4]. Within the mining industry, it is widely used to delineate paleochannels, map iron ore deposits, and image kimberlites [5,6]. However, challenges such as antenna crosstalk, ground reflections, ambient noise, and signal attenuation limit data accuracy [7,8].

Signal attenuation, particularly in highly conductive soils such as clay or those with a high mineral content, remains a major constraint. Solutions include the use of low-frequency antennas for deeper penetration [9,10], advanced signal processing techniques such as wave migration and deconvolution [11,12], as well as the integration of multi-frequency GPR systems to balance resolution and depth [13,14]. Furthermore, deep learning models such as *DMRF-UNet* enhance radar data reconstruction and interpretation accuracy, thereby strengthening GPR's effectiveness in meeting the demands of the mining industry [15].

Modern Ground Penetrating Radar (GPR) systems now achieve penetration depths ranging from hundreds to thousands of meters, while maintaining decimeter-scale resolution, even within crystalline rock formations [16,17]. Geological mapping remains a primary application, facilitating the assessment of mineral resources. This method offers numerous advantages for the exploration of iron mineralization, particularly its high spatial resolution, enabling the precise detection of anomalies near the surface. It is highly effective in locating complex geological structures and mineralization at shallow depths (up to 30-40 meters) [18]. Compared to magnetometry, GPR provides more accurate localization of structures, especially in environments where mineralization does not significantly affect the magnetic field. Magnetometry, however, is more suited for detecting large iron mineralization's but has a lower resolution [19]. Regarding resistivity, while GPR provides real-time imaging of the geological structure, resistivity can offer superior penetration in conductive soils [20]. Therefore, GPR is ideal for surface exploration, while resistivity proves more useful for deeper investigations. A combination of both methods may be necessary for a comprehensive subsurface analysis [21]. Although GPR is more expensive than magnetometry and resistivity, it offers superior precision and resolution, which can justify its higher cost in certain situations. Its primary advantage lies in its ability to provide real-time, high-resolution images of geological structures, enabling the precise detection of shallow anomalies and mineralization [22]. Unlike magnetometry, which is better suited for detecting large mineral concentrations and has lower resolution [23], or resistivity, which often requires complex modeling for data interpretation [24], GPR offers greater flexibility and accuracy in complex geological environments. Therefore, when the geological context warrants it—particularly for surface exploration or the detection of shallow mineralization—the higher cost of GPR can be offset by the quality and speed of the data obtained, ultimately op-

timizing long-term exploration operations.

This study presents the results of a GPR survey in the Nador region, aiming to optimize surface mining operations and reduce exploration costs through enhanced geological mapping [25].

To improve GPR efficiency in complex geological environments, several strategies can be implemented. Low-frequency antennas enhance penetration, while increased transmitter power mitigates signal attenuation [26]. Advanced filtering and inversion algorithms refine imaging [27], and multi-offset GPR with polarization variability adapts responses to subsurface conditions [28]. Technologies like Frequency-Modulated Continuous-Wave (FMCW) and multi-frequency GPR enhance spectral analysis, optimizing depth-resolution balance [29]. Field testing and wave-soil interaction models further refine parameter calibration and data interpretation [30].

For small-scale mining, automated software like *Micromine* and *GPR Insights* streamlines data processing. Preconfigured solutions and automated reporting facilitate rapid decision-making on-site.

GPR has proven effective in gold exploration by detecting sediment and bedrock anomalies [31], copper prospecting by identifying copper-rich veins [32], and geological mapping by delineating rock fractures [33]. GPR can be used to identify small alluvial iron deposits by detecting anomalies in near-surface soil layers, particularly in shallow mineralization [34]. However, its ability to detect fine-grained ferruginous rocks depends on factors such as soil composition and moisture content and may be limited in highly conductive soils [35]. Case studies from Australia and Brazil have demonstrated that GPR can successfully locate shallow alluvial iron deposits, although its effectiveness varies depending on geological conditions [36,37].It is also used in diamond exploration and sand dune imaging, with recent instrumentation advancements enhancing deep data acquisition in diverse environments [38,39]. Compared to other methods, GPR offers superior resolution, cost efficiency, and non-destructive analysis, though specialized expertise and software remain necessary for accurate data processing [38,40,41].

Optimizing results requires selecting suitable antennas, adjusting frequencies, and calibrating radar parameters [16,43]. Despite challenges from heterogeneous soils and iron ore-mud mixtures, this study assesses GPR's effectiveness in such conditions, contributing to humanitarian efforts. The primary objective is to locate buried structures and objects within residual deposits and mud in eastern Morocco [44].

2 Location and Description of the Study Area

Nador, located in eastern Morocco at coordinates 35° 10' 12" N, 2° 55' 48" W (Figure 1), is near the Beni Bou Ifrour massif, which is a basement window emerging from Neogene basins in the eastern Rif. This massif includes some of the most significant iron deposits in eastern Morocco, with over 60 Mt exploited from 1915 to 1976.

The Ouiksane deposit, notable for its high iron content (up to 70%), is the most significant among the three studied deposits. Located in the western sector of the North Domain of Beni Bou Ifrour, it is enclosed within a monoclinal series of east-west oriented shales with a northern dip, where the main carbonate bank is interbedded. The deposit is centered

around the Central Intrusion, a granodioritic pluton that forms a sub-concordant sill within the schist-carbonate bank contact. The intrusion caused contact metamorphism, transforming the surrounding limestones into marbles and the shales into corneans or skarns, depending on their initial lithology. Surface mining has created an open pit divided into two sections (open pit E and open pit W) by the Ouiksane fault [45]. The northern side of the pit exposes the intrusion, while the southern side reveals the host rock in front of the intrusion (Figures 2a and 2b) [46].

Figure 1. Location Map of the Study Area.

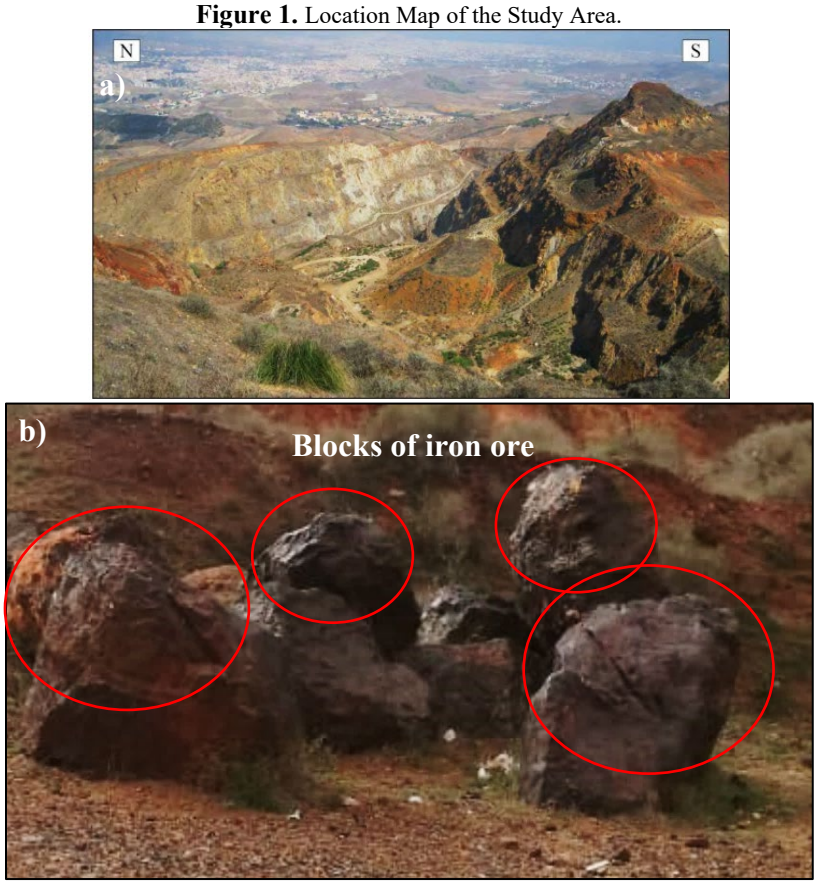

Figure 2. Panorama on the oriental open pit of Ouiksane and (b) some of the blocks of iron ore in this area.

The historical exploitation of Ouiksane iron has led to extensive mining studies, including comprehensive geological maps (Figure 1) and detailed cross-sections of the mine (Figure 2).

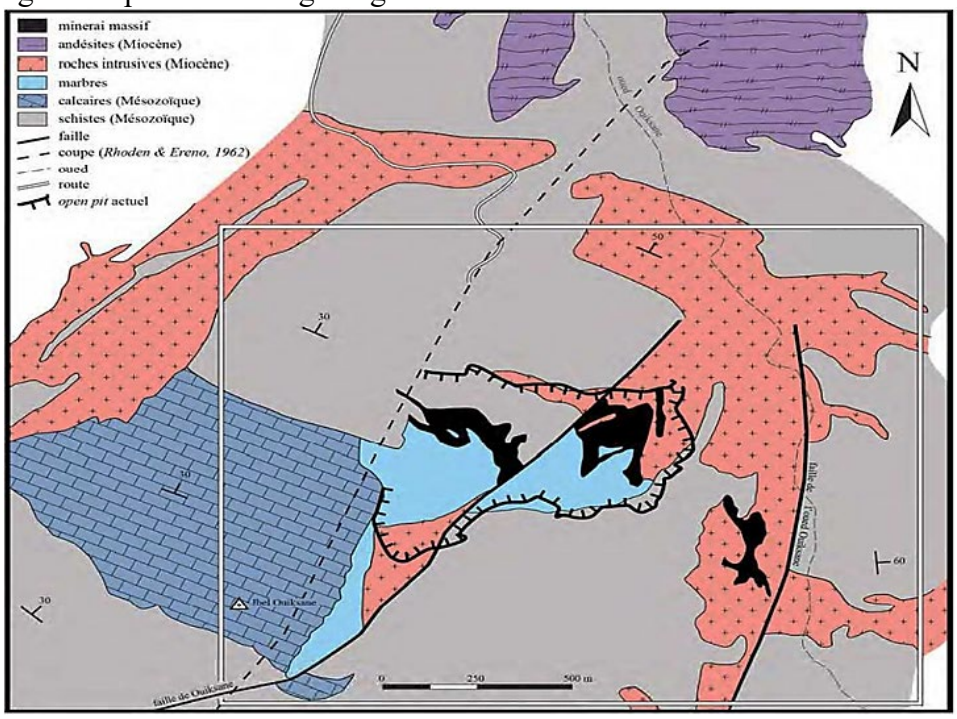

Figure 3. Historical geological map at the level of the Ouiksane deposit [19].

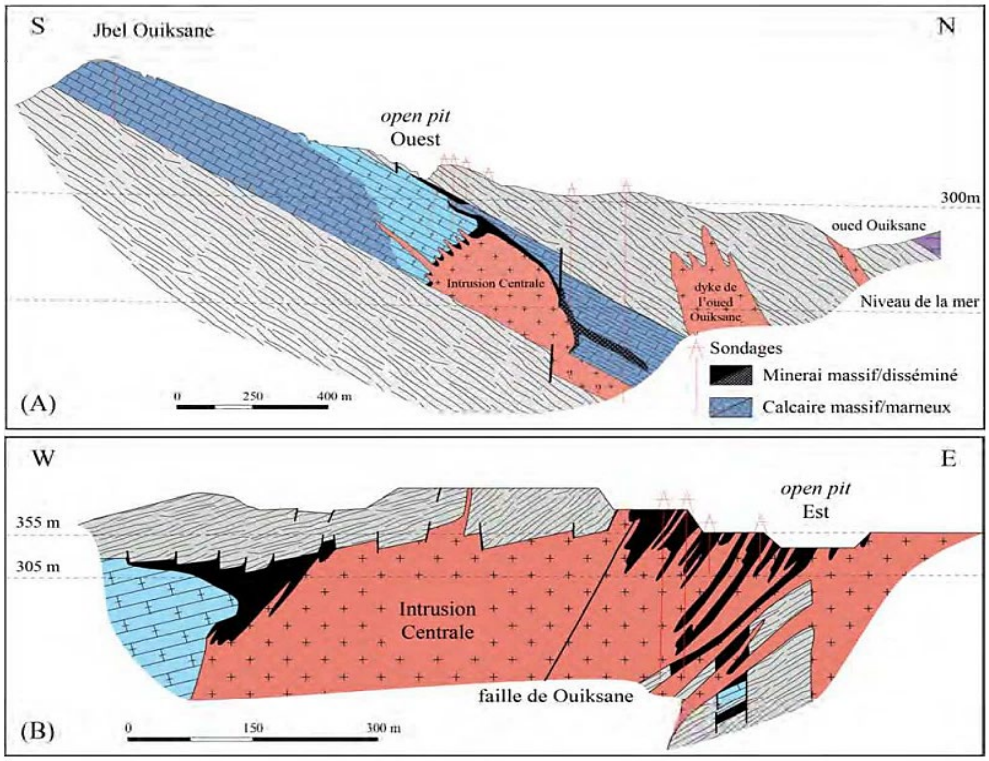

Figure 4. Historical geological sections explaining the structure of Ouiksane deposit [19].

3 Materials and Methodology

Ground Penetrating Radar (GPR) consists of a transmitter and receiver antenna, with their separation distance varying based on frequency and GPR type. This method transmits high-frequency electromagnetic waves (10-2600 MHz) into the subsurface and records reflected energy from different interfaces [47,48].

The receiver, equipped with an amplifier, enhances the reflected signals' amplitude. Antennas are designed to cover extensive areas in a single pass, and the use of multiple receivers allows for data "stacking," which improves the signal-to-noise ratio. The transmitter sends energy pulses into the subsurface, while the receiver detects reflections from interfaces between materials with different electrical properties [49,50]. GPR data interpretation relies on three key physical properties of the medium or buried targets: permittivity (ε), permeability (μ), and conductivity (σ) [51,52].

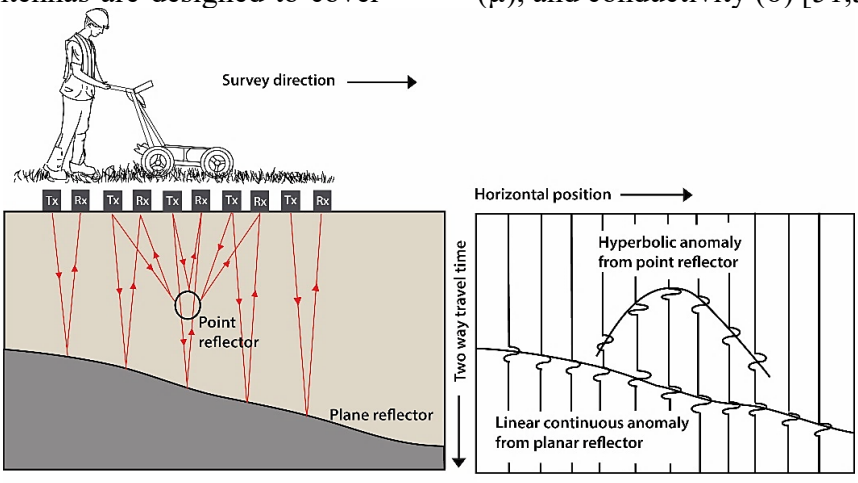

Figure 5. Principle and measurement of GPR Profile using constant-offset.

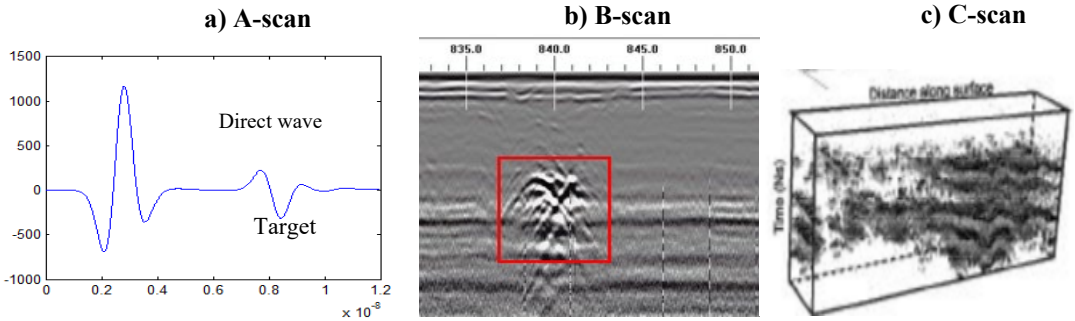

Figure 6. Typical signal, received by the GPR.

In the second stage of GPR operation, the receiving antenna captures the reflected waves, which are subsequently recorded and displayed as raw data in three formats: A-scan, B-scan, and C-scan, as depicted in Figure 6.

This section explores theoretical analyses essential for GPR operation, data interpretation, and detection of buried objects. Key parameters include the wave velocity in a homogeneous medium and its speed when interacting with a target. Additionally, it involves calculating the permittivity of both the medium and buried objects, as well as studying attenuation and reflection.

One of the key methods in radar exploration and data collection is constant-offset prospecting, illustrated in Figure 5. In this method, the transmitter and receiver antennas move simultaneously on the surface, maintaining a fixed distance that depends on the frequency used. Often, the propagation velocity must be estimated non-invasively from the GPR data itself.

The most prevalent approach for this estimation involves analyzing diffraction curves, or diffraction hyperbolas. This technique starts with a point-like target, i.e., a small buried object relative to the wavelength in the soil, as depicted in Figure 7.

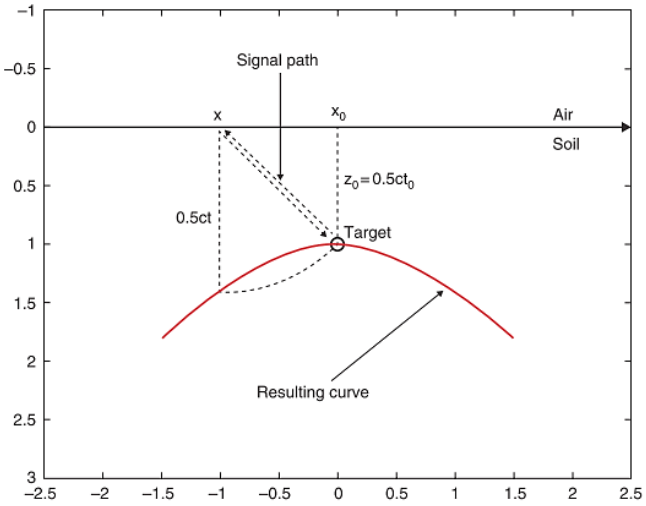

Figure 7. Measure of the permittivity of the soil from a diffraction hyperbola from a point-like target.

The transmitting antenna illuminates the target not only when it passes exactly over it, but also from a certain distance before it and up to a certain distance beyond it. So, the receiving antenna gathers an echo from the target not only when it crosses over it, but usually within a segment centered on the target. The length of this segment depends on the directivity of the antennas, the characteristics of the soil, and the depth of the target. If the antennas are moved at the air – soil interface, and the offset between them is neglected, then the distance from the position of the source-observation point (x,0) and the buried target in the position (x_0, z_0) is given by $\sqrt{(x-x_0)^2+z_0^2}$. This quantity corresponds to the apparent depth at the abscissa x, which in terms of propagation velocity is given by z(x) = ct /2, where t = t(x) the return time of the echo recorded at the position x. In the point x = x_0 , the apparent depth of the target reaches its minimum value z = z_0 = ct_0 /2, where t0 is the minimum recorded return time. Putting together these equalities, we have

$$\frac{ct}{2} = \sqrt{(x-x_0)^2 + \left(\frac{ct_0}{2}\right)^2}$$

$$t = \frac{2}{c}\sqrt{(x-x_0)^2 + (ct_0/2)^2}$$

$$\frac{t^2}{t_0^2} - \frac{(x-x_0)^2}{0.25c^2t_0^2} = 1 \qquad (1)$$

Relationship (1) is the equation of a hyperbola (but of course only one of the two branches is considered) with the vertex at the target position (x_0, t_0). Eq (1) is parametric with respect to the propagation velocity c, and so c can be estimated from Eq. (1). In principle, this might be done even just from two points, but of

course, a more extended fitting provides a more reliable result. There are commercial codes that allow us to do this fitting in an immediate graphical way [53,54] by depicting the model diffraction hyperbola at variance of a trial c on the data. As it is well known, by replacing 1 with 0 in the second term of Eq (1) we achieve the equation of the asymptotes of the hyperbola, that is,

$$t = \pm\frac{2}{c}(x - x_0) \quad (2)$$

The strength of GPR reflection in perpendicular incident waves depends on the contrast in relative dielectric constant across the reflecting boundary, while the reflection coefficient RC can be expressed as [55]:

$$RC = \frac{\sqrt{\varepsilon_{r1}}-\sqrt{\varepsilon_{r2}}}{\sqrt{\varepsilon_{r1}}+\sqrt{\varepsilon_{r2}}} \quad (3)$$

Where, $\varepsilon_{r1}$and ε_{r2} are the relative permittivity of medium 1 and 2 respectively. These values allowed the calculation of the dielectric constant ε_r according to the equation (3), where c is the speed of light (0.3 m/ns) and h is the depth :

$$z = \frac{Vt}{2} \quad (4)$$

$$V = \frac{c}{\sqrt{\varepsilon_r}} \quad (5)$$

$$\varepsilon_r = (\frac{ct}{2h})^2 \quad (6)$$

where C is the propagation speed of EM waves through air, which is equivalent to the speed of light, or 0.3 m/ns). As the wave propagates through material 2, its energy is attenuated as follows:

$$\alpha = 12.863\times10^{-8} f\sqrt{\varepsilon_2}(\sqrt{1+\tan^2\delta}-1)^{1/2} \quad (7)$$

where α attenuation, in decibel/meter, f wave frequency, in Hz, and δ= the loss tangent (or dissipation factor) is related to σ, the electrical conductivity (in mho/meter) of the material by:

$$\tan\delta = 1.80\times10^{10}\frac{\sigma}{f\varepsilon_2} \quad (8)$$

When the remaining microwave energy reaches another interface, a portion will be reflected through material 2 as given by Equation 3 [56,57].

Effective exploration and evaluation of underground minerals with GPR necessitate selecting appropriate instrumentation and understanding the soil type and its physical properties beforehand. This ensures the choice of suitable equipment and defines the target depth. For this study, based on the soil type, a 200 MHz antenna and a GPR SIR 3000 radar from GSSI were selected (Figure 8).

Figure 8. Antenna (200MHz) and GPR SIR 3000.

Table 1. Typical (approximated) values of conductivity and real dielectric

Materiel	ε	σ	v(cm)	λ (cm)	δ
Cavity (air)	1	0	30	75	0
Clay (wet)	12	0.1	8.52	21.29	5.35
Soil dray	2.5	0.00014	18.97	47.43	0.01
Sand dray	9	0.001	10	25	0.08
Sand	8	0.003	10.16	26.52	0.2
Water	81	0.01	3.33	8.33	0.21
Copper	1	5.6	2.62	6.55	95.52
Iron	1	1000000	0.01	0.02	39738.35

The GPR data were processed using Radan 7 and Reflexw to enhance the visualization of buried structures. Radan 7, developed by GSSI, offers modular tools for specific processing needs, intuitive 2D/3D visualizations, and includes key steps such as filtering and time-depth conversion. Reflexw is a versatile software used for GPR, seismic, and ultrasound data, featuring 2D and CMP velocity analysis modules, as well as a wide range of processing options like filters, gains, interpolation, and advanced migration techniques.

4 Results and data analysis

4.1 Detection targets by GPR modelling

Various commercial programs are employed to simulate radar signals for detecting buried objects. In this study, we utilize the GprMax2d software, developed by Giannopoulos in 2005, which is available online and has been updated for scalability and enhanced functionality. This program operates based on the Finite-Difference Time-Domain (FDTD) method and integrates well with specific requirements. We employed this algorithm to improve the accuracy of object detection and to analyze their physical properties and geometrical shapes. For this modeling exercise, we simulated three targets with varying physical properties (dielectric, perfect dielectric, and conductor) and rectangular geometrical shapes (50 x 20 cm).

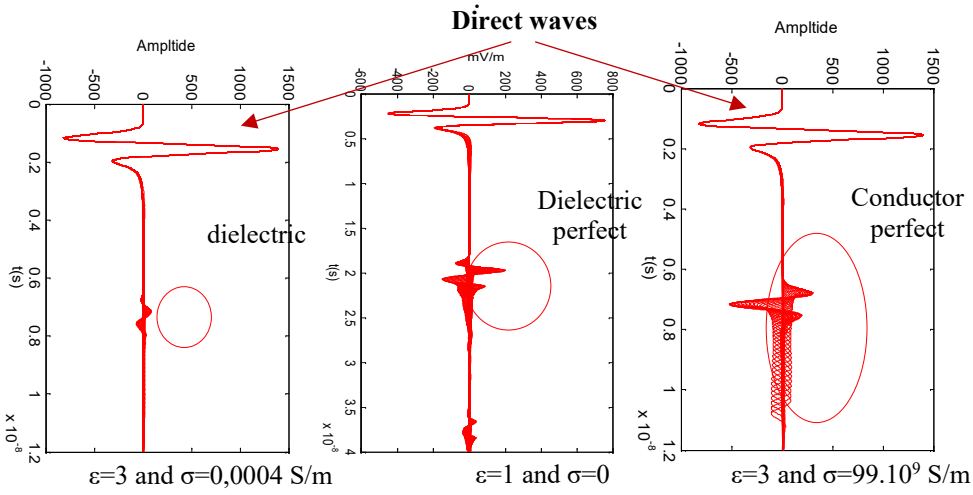

Figure 9. The amplitude of the signal reflects from the rectangular targets L=50cm and w=20cm (a) reflect from target dielectric, (b) reflect from target perfect dielectric and (c) reflect from target perfect conductor.

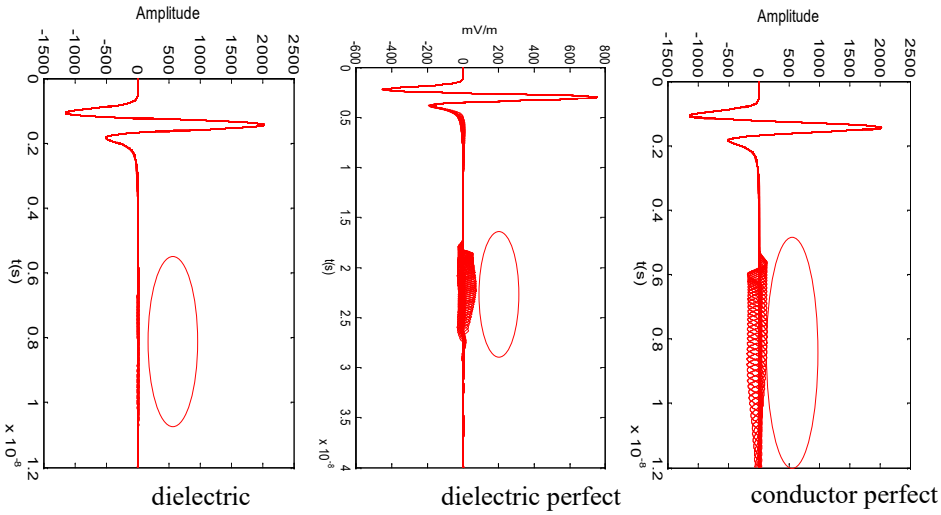

Figure 10. The amplitude of the signal reflected from the circular targets R=10cm (a) reflected from target dielectric, (b) reflected from target perfect dielectric and (c) reflected from target perfect conductor.

In Figure 9 and 10, we will simulate spherical targets with different physics properties, dielectric, perfect dielectric, and perfect conductor.

Modeling simulations using GPRMax rely on idealized conditions, which can limit the accuracy of results in real geological environments. These models often assume a homogeneous and isotropic medium, whereas the subsurface exhibits natural heterogeneities (such as fractures, permittivity variations, and the presence of fluids) that significantly influence the propagation of electromagnetic waves. Furthermore, the boundary conditions imposed in simulations often oversimplify complex phenomena, including multiple reflections and signal attenuation. As a result, discrepancies between theoretical responses and actual field measurements can be substantial, necessitating rigorous experimental validation. Therefore, integrating field data and refining model parameters are crucial to enhancing the reliability of GPR-based geophysical interpretations.

To improve the penetration depth of GPR, several studies suggest the use of low-frequency antennas, which offer better penetration in resistant soils such as clays by reducing attenuation losses [58]. In parallel, advanced numerical models that account for complex parameters such as subsurface heterogeneity and anisotropy have improved the accuracy of simulations, considering local variations in permittivity and conductivity of materials [59]. Furthermore, field tests in various geological contexts, such as drilling formations and cavities, are crucial for validating models and refining theoretical simulations by adjusting parameters based on real-world conditions [60]. Integrating these approaches could greatly enhance the reliability of GPR in diverse geological environments.

Other simulations were conducted to study the variation in the amplitude of the reflected signal from the Ground Penetrating Radar (GPR) when detecting iron deposits, analyzing the impact of different frequencies (800 MHz, 400 MHz, and 200 MHz) on signal reflection and the differences in the received signals.

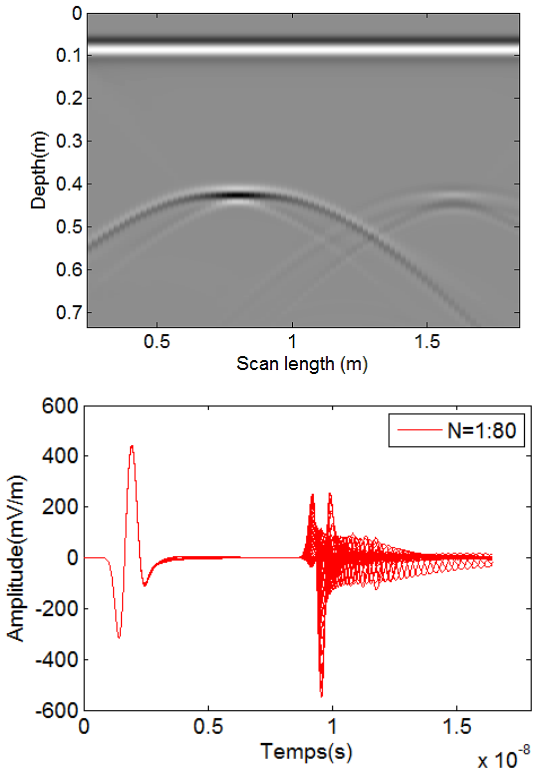

Figure 11. Variation of the reflected signal amplitude over time with an antenna of frequency f = 800 MHz and analysis of the received signals.

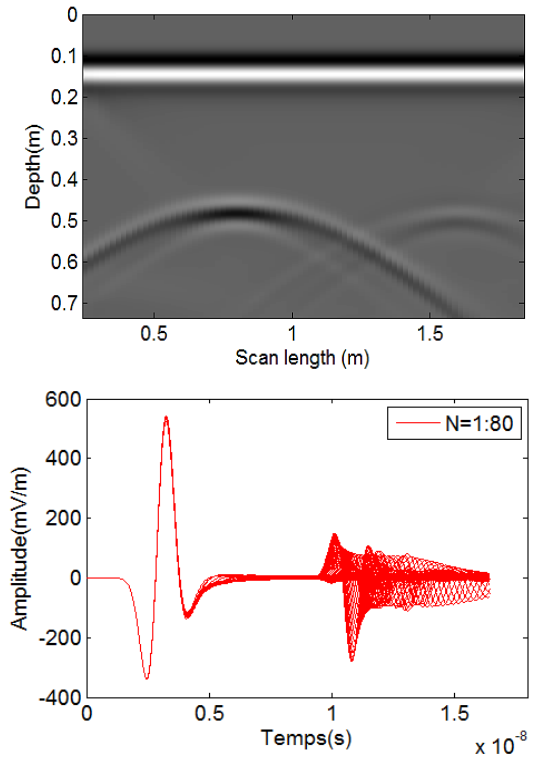

Figure 12. Variation of the reflected signal amplitude over time with an antenna of frequency f = 400 MHz and analysis of the received signals.

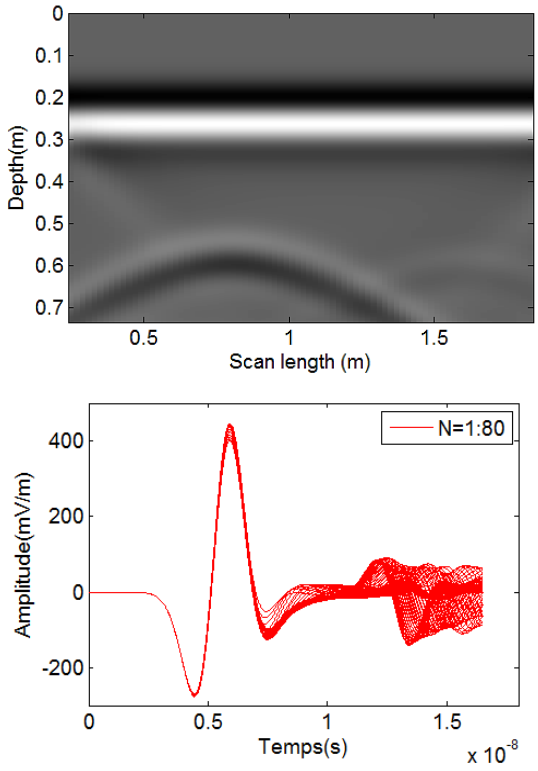

Figure 13. Variation of the reflected signal amplitude over time with an antenna of frequency f = 200 MHz and analysis of the received signals.

The variation in the amplitude of the reflected signal, measured using antennas with different frequencies (800 MHz, 400 MHz, and 200 MHz), depends on the depth of the iron deposits. At 800 MHz, the radar provides high resolution for detecting shallow deposits but has limited penetration (Figure 11). At 400 MHz, it offers a good compromise between resolution and depth, making it suitable for deposits at moderate depths (Figure 12). At 200 MHz, penetration is increased, allowing for the detection of deeper deposits, but with less precise resolution (Figure 13). For our case study, the 200 MHz antenna was chosen to maximize the detection of deeper deposits due to its superior penetration capability.

4.2 Experimental Results with 200MHz

To carry out the anomaly survey and site investigation, the area was divided into four sections, each ranging from 30 to 40 meters in length, with a 2-meter spacing between each profile.

GPR Profiles in zone 1.

Key factors in interpreting GPR data include the hyperbolic shape of signals, attenuation, reflection coefficient, and wave velocity. Radargram 1 in Figure 14, using a 200 MHz antenna, shows multiple hyperbolas resulting from reflections on the surface of an iron block. A target is identified at a depth of 2 meters, with dimensions of 16 meters in length and 1.6 meters in thickness. The antenna effectively penetrated up to 6 meters.

Significant anomalies are observed between 55 and 71 meters, at depths of 2 to 4 meters, marked by high-amplitude

reflections. This contrasts with the attenuated signals in other radargrams. A constant wave amplitude from 0.1 to 2 meters suggests a homogeneous medium, while variations from 2 to 5 meters indicate a heterogeneous medium, likely containing objects or cavities. Repeated hyperbolic segments and high signal amplitude in Zone 1 suggest the presence of iron ore blocks with high conductivity and low permittivity.

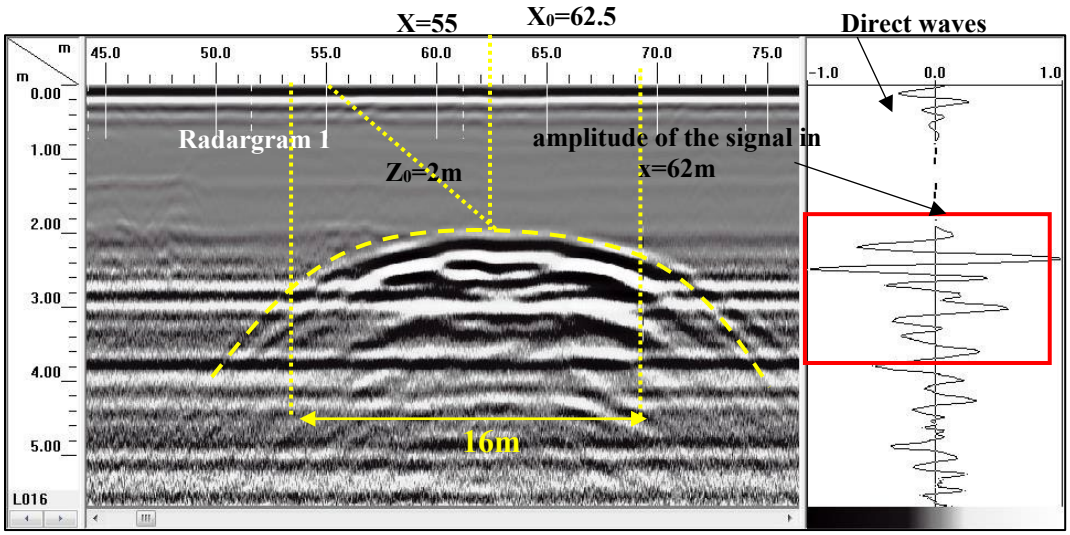

Figure 14. Radargram 1 of profile 1 in zone 1 shows the data obtained during the investigation and search in the Nador region using a 200 MHz antenna.

Radargram 2 (Figure 15) shows similar high-amplitude reflections at depths of 2 to 4.5 meters, consistent with other radargrams.

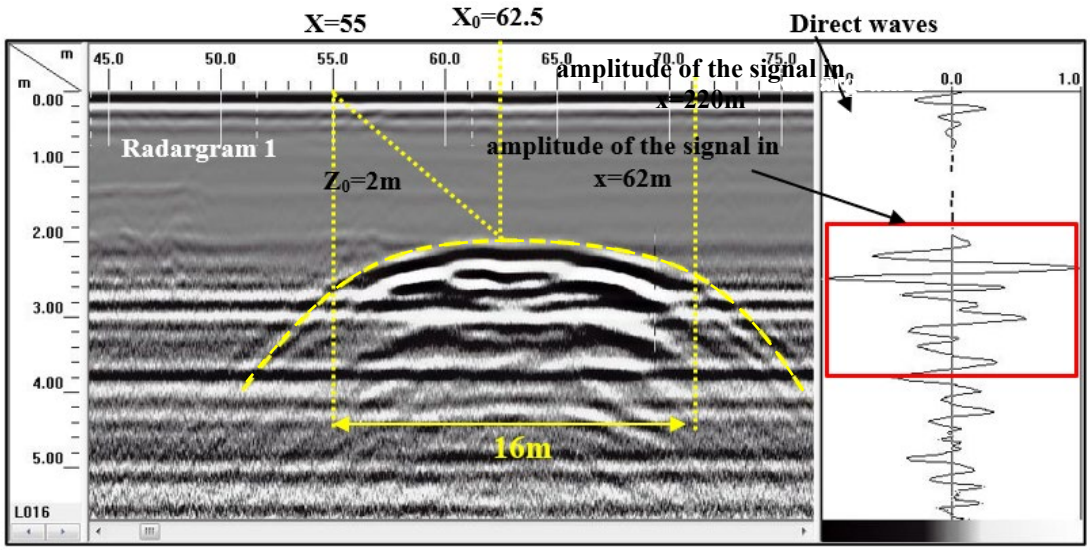

Figure 15. Radargram 2 of profile 2 in zone 1 shows the data obtained during the investigation and search in the Nador region using a 200 MHz antenna.

GPR Profiles in zone 2.

In Zone 2, the radargram reveals multiple hyperbolas resulting from the reflection of waves on the surface of an iron block (Figure 16). The profile in Figure 14 shows abnormally high reflections between 390 and 427 meters (37 to 40 meters in length). Depths ranging from 2 to 6 meters are highlighted in the enclosed area.

The observation of the radargram and the repetition of hyperbolas, along with the signal amplitude, as illustrated in Figure 14, indicate that the detected objects have very high conductivity and very low permittivity, suggesting the presence of pure iron.

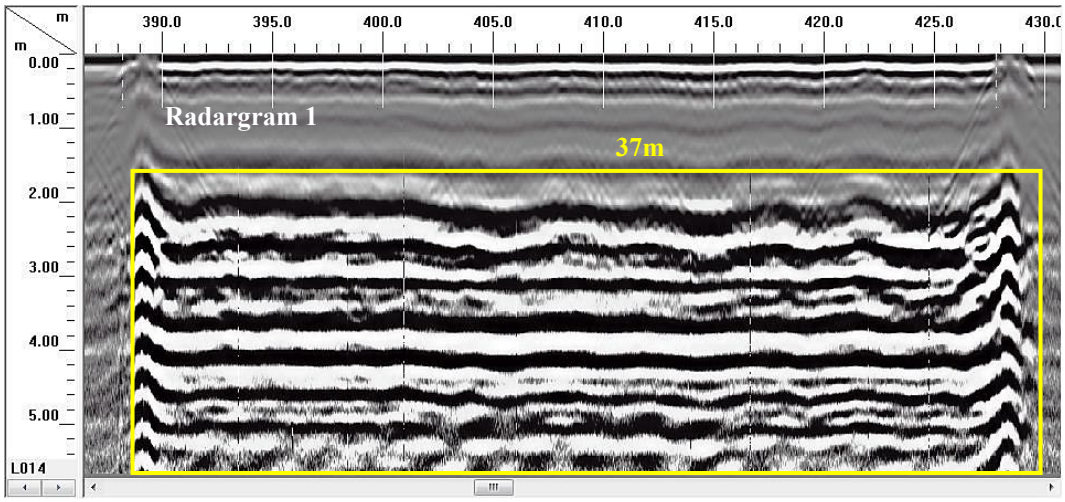

Figure 16. 0Radargram of profile 1 in zone 2 shows obtained data by investigation and search in Nador region using 200 MHz antenna, explains the appearance of minerals.

The same observation was repeated; Figure 17 demonstrated an excellent subsurface penetration capacity at a depth of 6 meters. This profile revealed anomalous and very high-amplitude reflections between 515 and 560 meters in radargrams 1 and 2.

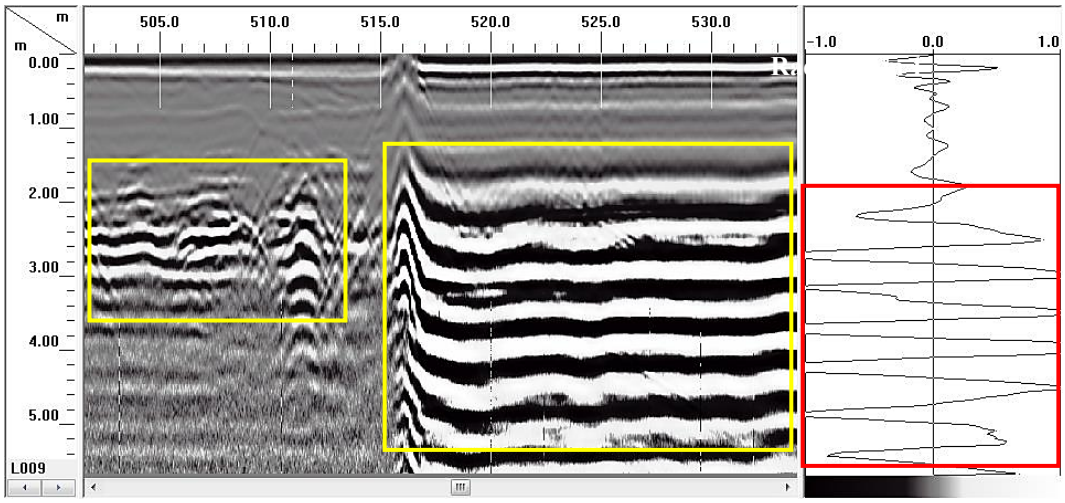

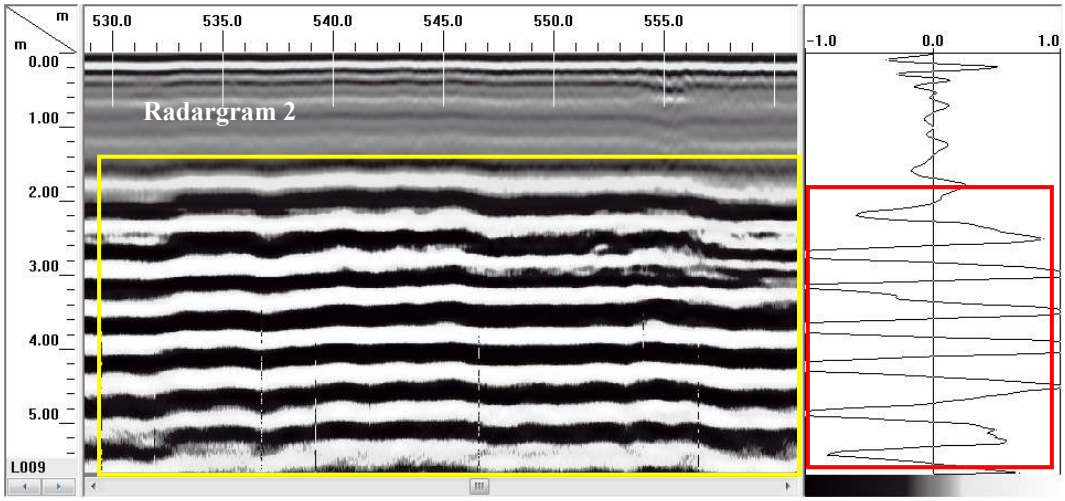

Figure 17. Radargram of Profile 2 in Zone 2 showing the presence of minerals.

GPR Profiles in zone 3.

The profiles in Zone 3 revealed abnormal reflections, clearly identifiable in the radargrams (highlighted area), while the signal was strongly attenuated in the rest of the radargrams. In this region, we observe the presence of anomalies in the Earth's layers, as well as heterogeneity indicating a contrast, which explains the appearance of minerals and changes in the Earth's layers. In Zone 3, we observe the recurrence of deformations that extend in profiles 1 and 3 between 480 and 510 meters.

The radargram of Profile 4 (Figure 20) shows repeated distortions and the appearance of certain bodies that have been confirmed to be minerals.

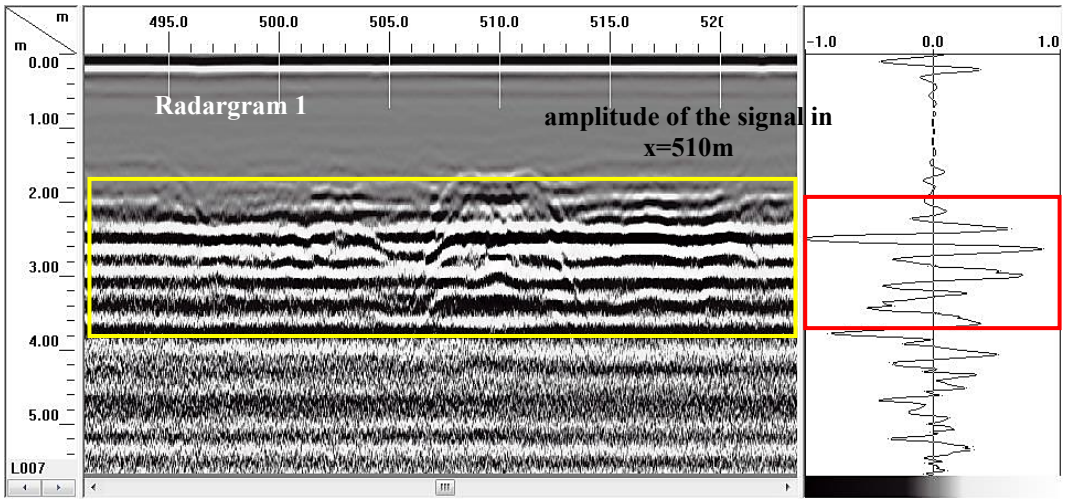

Figure 18. Radargrams of profile 1 in zone 3 explain the appearance of minerals and changes in the Earth's layers.

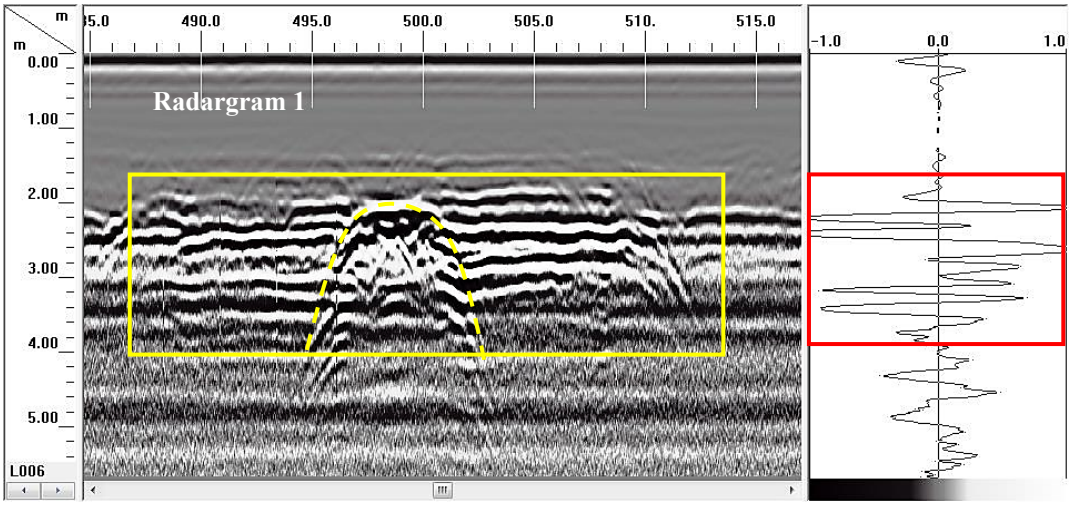

Figure 19. Radargrams of profile 2 in zone 3 explain the appearance of minerals and changes in the Earth's layers.

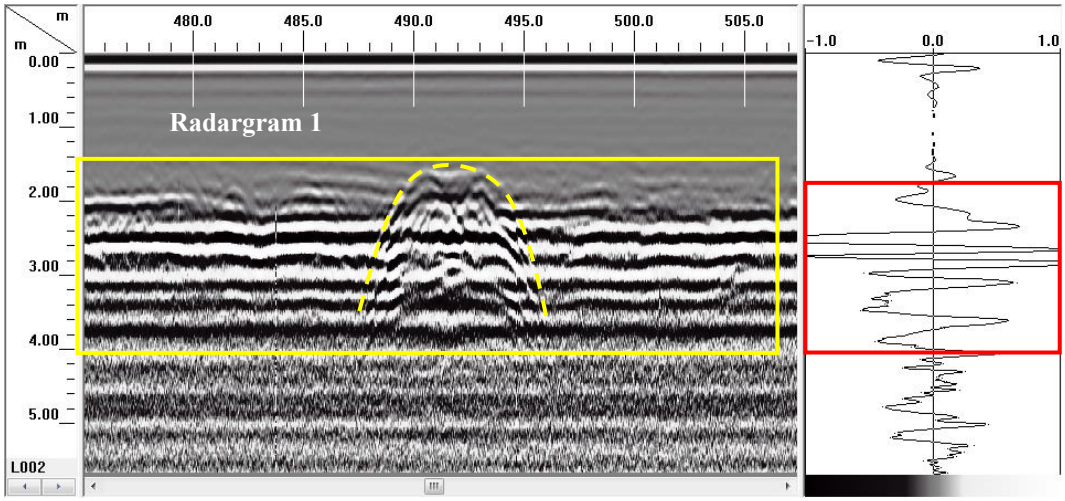

Figure 20. Radargrams of profile 3 in zone 3 explain the appearance of minerals and changes in the Earth's layers.

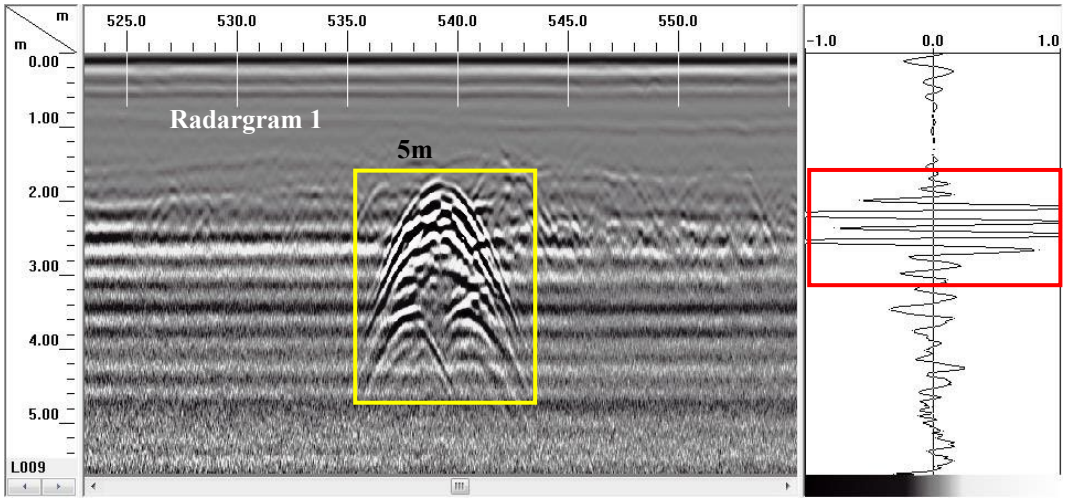

Figure 21. Radargram of Profile 4 in Zone 3 showing the presence of minerals.

GPR Profiles in zone 4.
Figure 22 illustrates the results of the GPR profile in Zone 4. This profile revealed an abnormally clear reflection over a length of more than one kilometer and at depths ranging from 2 to 6 meters. It is important to note the attenuation of the signal in the radargrams. We observe that hyperbolic GPR signals are nonexistent in zone 4, which could indicate very wet soil or the presence of water at a great depth, as shown in Figure 22.

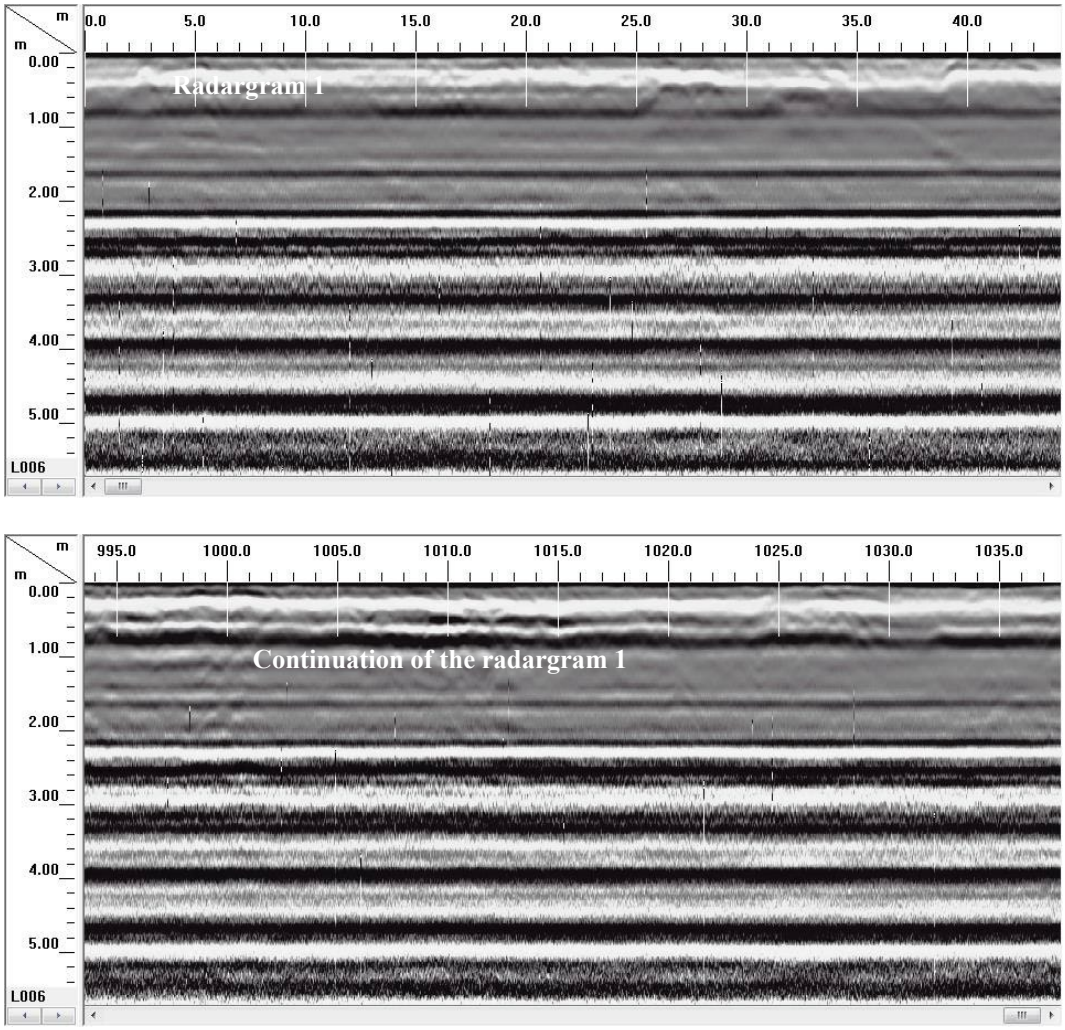

Figure 22. Radargram of profile 1 in zone 4.

5 Conclusion

The results of the survey and exploration by GPR (GSSI SIR 3000 system) with 200 Mhz antenna were very successful and surprising in identifying and detecting iron ores as well as studying the underground. It was also successful in penetrating lands with difficult and muddy conditions. Iron ore deposits often exhibited very low conductivities rendering them ideal candidates for GPR resource evaluations. Although these deposits are often hundreds of meters in depth, GPR systems were high-resolution in the first 7m, variations that are not readily detected by drill grids. Radar GPR is an effective and successful technology of searching as well as easily detecting underground minerals, less expensive and without excavation. Also, by radar GPR,

we can make geological maps of the Earth's layers and sub-surface components. In this work, we were successful and able to uncover many metal blocks of different sizes and different depths and several GPR profiles have been carried out along across these zones.

References

Benassi, R.F., et al. "Wave Migration and Deconvolution Techniques for Improved GPR Imaging." Geophysical Prospecting, 68(5), 1205-1217, 2020.

Botha, G.A., et al. "Evidence for Dune Reactivation from Ground Penetrating Radar (GPR) Profiles on the Maputaland Coastal Plain, South Africa." Ground Penetrating Radar: Applications in Sedimentology, Geological Society, London, Special Publications, 211, 26-46, 2003.

Boev, G., and Angelov, R. "GPR Investigation for the Detection of Buried Metal Structures in Mining Operations." Journal of Applied Geophysics, 93, 130-141, 2013.

Chen, Y., Yang, X., and Zhang, T. "Multi-Offset Ground Penetrating Radar System for High-Conductivity Environments." Geophysics, 83(4), 1-12, 2018.

Cheng, J.L., Hu, K., Wang, Y., and Cao, J.S. "Research on Detecting Underground Mined-Out Areas Using GPR." Rock and Soil Mechanics, 25, 79-82, 2004.

Cheng, X. "Comparison of Ground Penetrating Radar and Magnetometry for Mineral Exploration." Exploration Geophysics, 35(4), 123-132, 2004.

Conyers, L.B. "Ground-Penetrating Radar for Archaeology." Altamira Press, 2013.

Davis, R., et al. "Field Validation of GPR in Complex Geological Environments." Journal of Applied Geophysics, 60(2), 2019.

Francke, J. "A Review of Selected Ground Penetrating Radar Applications to Mineral Resource Evaluations." Journal of Applied Geophysics, 81, 29-37, 2012.

Francke, J., and Utsi, V. "Advances in Long-Range GPR Systems and Their Applications to Mineral Exploration, Geotechnical and Static Correction Problems." First Break, 27(7), 2009.

Francke, J., and Yelf, R. "Applications of GPR to Surface Mining." 2nd International Workshop on Advanced Ground Penetrating Radar, 115-119, 2003.

Francke, T. "Ground Penetrating Radar (GPR) Applications in Mineral Exploration." Journal of Applied Geophysics, 83(2), 129-135, 2012.

Fischer, M., et al. "A Novel Ground Penetrating Radar System for High-Resolution Mapping of Underground Ore Bodies." Geophysics, 80(5), B163-B174, 2015.

Gatti, P.L., et al. "Performance of Low Frequency Antennas for Ground Penetrating Radar in Highly Conductive Materials." Near Surface Geophysics, 15(6), 533-542, 2017.

Gibson, M.D. "Ground Penetrating Radar with FMCW for Geological Surveying." Journal of Environmental and Engineering Geophysics, 23(2), 121-130, 2018.

Goodwin, T., and Garcia, R. "GPR for Subsurface Mapping in Mining and Archaeological Contexts." Geophysics, 80(5), 193-206, 2015.

Guérin, C., et al. "Mapping of Buried Infrastructure and Material in Mining Sites with GPR." Geophysical Journal International, 205(1), 345-360, 2016.

Harris, J.D., et al. "Ground Penetrating

Radar in Iron Ore Exploration in the Australian Outback." Journal of Geophysical Research, 118(10), 3506-3517, 2016.

Hogan, G. "Migration of GPR Data: A Technique for Locating Subsurface Targets." In Proceedings of the Second International Symposium on Geotechnical Applications of Ground Penetrating Radar, West Gainesville, Florida, March 6-10, 1988, U.S. Dept. of Agriculture, Washington, DC, 164-179, 1988.

Jha, P.C., et al. "GPR Applications in Mapping Barrier Thickness in Coal Mines: Some Case Studies." Proceedings of the Tenth International Conference on Ground Penetrating Radar, GPR 2004. IEEE, 2004.

Johnston, G., and Slater, L. "Analysis of Ground Penetrating Radar Data for Assessing Soil Conditions in Mining Areas." Soil Science Society of America Journal, 72(3), 865-875, 2008.

Johnson, M., et al. "Advanced Numerical Modeling of GPR in Heterogeneous Media." Elsevier Geophysics Journal, 23, 2020.

Johnson, P., and Lee, M. "Mapping Rock Fractures Using GPR for Improved Mining Operations." Journal of Structural Geology, 59(4), 112-118, 2018.

Koster, B., and Kruse, F. "The Use of Ground Penetrating Radar (GPR) in the Investigation of Historical Quarry Abandonment in Svalbard." Polar Record, 52(3), 330-344, 2016.

Kutrubes, D.L. "Dielectric Properties of Complex Media as Pertains to the GPR Technique." Geophysics Journal, 72(8), 431-450, 2018.

Maud, R.R., and Botha, G.A. "Deposits of the Southeastern and Southern Coasts." In The Cenozoic of Southern Africa, edited by Partridge, T.C. and Maud, R.R., Oxford University Press, 19-32, 2000.

Matthews, A.S., and Sims, M.R. "Effectiveness of GPR in Soil Exploration: A Case Study of Mineral Identification." Geophysical Prospecting, 62, 455-470, 2014.

McNeill, J.D., and Schell, W. "Ground Penetrating Radar Technology for the Mining Industry." Proceedings of the Third International Symposium on Geotechnical Applications of Ground Penetrating Radar, 87-95, 1990.

Morozov, C.P., Savaliev, A.V., and Ezhov, I.S. "Advanced GPR Data Processing Using Wavelet Transform and Adaptive Filtering Techniques." Geophysics, 81(3), 1-10, 2016.

Oliveira, C.J.R.S., et al. "Low Frequency Ground Penetrating Radar for Improved Subsurface Imaging in Conductive Soils." Journal of Applied Geophysics, 180, 222-230, 2020.

Oliveira, C.L., and Souza, F.M. "Application of GPR for Mapping Alluvial Iron Ore Deposits in Brazil." Geophysics, 80(4), B163-B173, 2015.

Pellerin, L., and Liao, S. "GPR Surveying for Depth-to-Bedrock Mapping in Mining Exploration." Geophysical Prospecting, 56(3), 415-423, 2008.

Rachidi, F., et al. "Analysis of GPR Signals in Fractured Rock Formations for Mineral Exploration." Journal of Geophysical Research: Solid Earth, 121(7), 5045-5063, 2016.

Rao, Y., and Zuo, J. "GPR Signal Processing in Non-Destructive Testing of Mining Materials." Journal of Nondestructive Testing, 36(8), 1124-1134, 2017.

Reddy, S.K.S., and Rao, A.S. "Modeling of Radar Signal Interactions with Soil for Improved GPR Data Interpretation." IEEE Transactions on Geoscience and Remote Sensing, 58(6),

3967-3976, 2020.
Schrott, L., and Chalikakis, K. "Geophysical Methods for Subsurface Exploration: GPR and Resistivity." Geophysical Journal International, 182(2), 621-635, 2010.
Smith, J., and Brown, A. "Application of Ground Penetrating Radar for Gold Exploration in Alluvial Regions." Journal of Geophysical Exploration, 72(3), 205-210, 2019.
Smith, J., et al. "Improving GPR Depth Penetration with Low-Frequency Antennas for Subsurface Exploration." Geophysical Research Letters, 45(12), 2018.
Smith, R.B., et al. "Application of Ground Penetrating Radar for Mineral Exploration: A Review of Methods and Case Studies." Journal of Applied Geophysics, 112, 15-29, 2015.
Soliman, M.S., et al. "Techniques for Enhancing GPR Resolution in Dense Subsurface Environments." Geophysical Journal International, 187(1), 392-406, 2011.
Straser, V., et al. "Use of GPR for the Detection of Subsurface Rock Layers in Mineral Exploration." Geophysical Journal International, 195(2), 123-132, 2013.
Sun, Y., and Zhang, W. "GPR for Investigating Subsurface Structures in Deep Mining Applications." Geophysical Prospecting, 66(6), 1254-1267, 2018.
Telford, W.M., et al. "Applied Geophysics: Principles and Methods." Cambridge University Press, 2nd Edition, 1990.
West, A.M., and White, R. "Developments in Ground Penetrating Radar Applications to Ore and Rock Mapping." Journal of Exploration Geophysics, 78(5), 2017.
Yao, Y., et al. "Evaluation of Ground Penetrating Radar for Detecting Cracks in Concrete Pavements." Journal of Civil Engineering, 15(6), 729-738, 2015.
Zhang, L., and Zhang, S. "Use of GPR for Mapping of Subsurface Void Spaces in Mining." Geophysics, 79(4), 88-98, 2014.
Zhang, Y., et al. "Recent Advances in Ground Penetrating Radar Technology for Mineral Exploration." Journal of Applied Geophysics, 151, 115-124, 2020.
Zhao, Q., and Li, X. "Detection of Subsurface Mining Voids Using Ground Penetrating Radar." Geophysical Prospecting, 65(1), 61-72, 2017.
Ziegler, E., and Singh, R. "Development of Ground Penetrating Radar Techniques for High-Resolution Imaging of Underground Ore Bodies." Journal of Geophysics, 68(3), 167-179, 2014.
Zuo, Q., and Yang, X. "Ground Penetrating Radar for Monitoring Environmental Changes in Mining Areas." Geophysics, 83(4), 31-42, 2018.
Zubair, M., and Jia, Z. "Advances in GPR Technology and Its Applications in Surface Mining." Geophysics Journal, 33(9), 211-225, 2018.
Yao, J., and Zhang, L. "Applications of Ground Penetrating Radar in Engineering Geophysics." Chinese Journal of Geophysics, 60(10), 2887-2896, 2017.
Zhao, S., et al. "Improvement of GPR Systems for Deep Subsurface Exploration in Mineral Mining." Geophysical Research Letters, 43(7), 3209-3216, 2016.
Yuan, W., et al. "Use of GPR for Mapping Soil Layers in Mining Areas." Journal of Soil Science, 51(4), 867-876, 2016.
Wang, C., et al. "Applications of Ground Penetrating Radar for Geophysical

Prospecting in Mining Industry." Geophysical Journal, 43(5), 517-528, 2017.

Zhang, L., and Li, Y. "Modeling Ground Penetrating Radar Propagation in Complex Subsurface Environments." Geophysical Prospecting, 61(9), 99-108, 2017.

Zhang, W., and Liu, X. "High-Resolution Subsurface Imaging Using Ground Penetrating Radar in Mining Operations." Journal of Applied Geophysics, 121, 234-247, 2016.

Zhang, Y., and Xie, W. "Ground Penetrating Radar for Mapping Geological Structures in Mining Areas." Journal of Geophysical Research, 127(2), 539-548, 2020.

Zhao, L., et al. "Ground Penetrating Radar Imaging of Mining Voids: An Innovative Approach." Geophysical Journal International, 199(3), 1097-1112, 2019.